J. Electrochem. Sci. Eng. **15(6)** (2025) 2708; http://dx.doi.org/10.5599/jese.2708

Open Access : : ISSN 1847-9286
https://pub.iapchem.org/ojs/index.php/JESE

Original scientific paper

Design, fabrication and functional properties of titanium suboxide-based composites with low noble metal content for electrocatalytic applications

Valentina Knysh, Heorhii Zhemela, Olesia Shmychkova✉, Tatiana Luk'yanenko and Alexander Velichenko

Ukrainian State University of Science and Technologies, 2, Lazaryana Str., 49010 Dnipro, Ukraine
Corresponding author: ✉*o_shmychkova@ukr.net;* Tel.: +380563772974; Fax: +380563772974
Received: March 11, 2025; Accepted: September 8, 2025; Published: September 17, 2025

Abstract

Fabrication, design and investigation of functional properties of composite materials based on titanium suboxides with low noble metal content for use in electrocatalysis has been investigated. The study particularly focuses on electrode coatings derived from titanium dioxide modified with platinum and palladium. The structural, electrocatalytic, and corrosion-resistant properties of these materials were systematically investigated. It was demonstrated that thermal treatment significantly enhances the catalytic efficiency of the coatings by reducing the oxygen evolution overpotential and improving the efficiency of hypochlorite synthesis. Optimal thermal treatment conditions (500 °C, 3 hours) were identified, resulting in increased stability of the anodes containing Pt and Pd layers, as evidenced by a service life of 176 hours. The study highlights the potential of these composites for applications in oxygen evolution reactions and hypochlorite synthesis, owing to their high stability, selectivity, and cost-effectiveness.

Keywords

Titanium composites; precious metals; semiconducting properties; electrocatalysts; oxygen evolution reaction; hypochlorite synthesis

Introduction

A key objective in electrocatalysis is to predict and control catalytic activity based on a theoretical understanding of reaction mechanisms. Developing effective catalysts requires studying electrochemical processes on anodic materials with diverse properties to reveal links between composition, selectivity, and synthesis conditions, especially when side reactions reduce product purity.

Titanium dioxide (TiO_2) has attracted attention due to its unique properties: similar thermodynamics of polymorphs, strong Ti–O bonds, and low redox potentials. These enable its application in sensors [1], electronics [2] and catalyst support [3]. Titanium suboxides, with developed surfaces

and non-stoichiometric structures, offer promising electrocatalytic potential due to various defects like oxygen vacancies and interstitial cations [4,5].

These materials can be synthesized *via* anodizing titanium in ethylene glycol with NH_4F and water, followed by electrochemical reduction [6,7]. A combined method involves platinum electrodeposition on titanium, followed by heat treatment in an oxidizing atmosphere, which allows for the formation of a composite differing from traditional Ti/Pt anodes in composition and activity [8,9].

Palladium and its oxides offer favourable electrochemical properties, with lower overpotentials for chloride oxidation and higher for oxygen evolution reaction [10]. Given their similar costs, Pt-Pd composites are promising for reducing noble metal usage while maintaining performance and corrosion resistance.

The goal of this work is to obtain and evaluate the qualities of composites based on titanium suboxides with reduced noble metal content. Combining Pt and Pd on a titanium suboxide support and optimizing thermal treatment parameters (500 °C, 3 hours) is not entirely new but offers incremental innovation in terms of stability and electrocatalytic performance.

The innovative aspect of this work is the significant reduction in the content of platinum group metals in the coating compared to traditionally used Ti/Pt electrodes. This makes it possible to propose competitive materials with a low content of precious metals for applications such as cathodic protection of metal structures or electroplating, where minimizing the oxidation of electrolyte components is critically important. These types of materials can also serve as an alternative to traditional PbO_2- and SnO_2-based electrodes for pollutant oxidation, particularly in solutions with low chloride ion content.

Experimental

Titanium foil was utilized (Titanium Plus Ltd, Ukraine); ammonium fluoride, ethylene glycol, and phosphoric acid were obtained from Fluka (Switzerland); perchloric acid was purchased from Expert Q® (Spain). Chemicals were commercial products of at least reagent-grade.

Composite synthesis

The electrodes were prepared on pre-treated titanium foil (titanium grade VT1-0). The electrode surface was 4 cm^2. The procedure included several stages of pre-treatment of the titanium substrate [11]. The initial porous TiO_x substrate was obtained by anodizing titanium foil in ethylene glycol with the addition of 0.3 wt.% ammonium fluoride and 2 vol.% water for 3 hours (1st anodization). This was followed by anodization in ethylene glycol with 5 wt.% H_3PO_4 (2nd anodization). Reduction was carried out electrochemically in 1 M $HClO_4$ for 1 hour at a current density of 5 mA cm^{-2}, which led to charge redistribution in the lattice (a decrease in oxygen content) and an increase in the non-stoichiometry of the structure. Afterward, a non-continuous layer of palladium from a phosphate palladium plating electrolyte or a non-continuous layer of platinum from a nitrite platinating electrolyte [12] or sequential layers of platinum and palladium were layered onto the oxide. The weight of precipitated metals, determined gravimetrically, was 0.5 mg of metal per cm^2, depending on the experimental goals. Thermal treatment was carried out in air using a high-temperature SNOL 8.2/1100 TermoLab electric furnace at various temperatures and times.

Morphology and structural characteristics

The surface morphology was analysed on a Tescan Vega 3 LMU microscope, which is equipped with an Oxford Instruments Aztec ONE energy-dispersive X-Ray microanalyzer and an X-MaxN^{20} detector using scanning electron microscopy (SEM) and energy dispersive X-ray spectroscopy

techniques. The structural characteristics of the coatings were investigated through powder X-ray diffraction. The diffraction data were obtained using a STOE STADI P automated diffractometer with a linear PSD detector, operating in transmission mode with $2\theta/\omega$ scanning. The setup included Cu Kα1 radiation, a curved germanium (1 1 1) monochromator, a 2θ range from 6.000 to 102.945° with a step size of 0.015°, a PSD step of 0.480° and a scan duration of 50 s per step.

Initial data processing and qualitative phase analysis of the X-ray diffraction patterns were carried out using the STOE WinXPOW and PowderCell software packages. The crystal structures of the phases were refined using the Rietveld method in the FullProf.2k program, employing a pseudo-Voigt profile function and an isotropic model for atomic displacement parameters. In addition, microstructural parameters – namely, the average apparent crystallite size D (derived from the size of coherently diffracting domains) and the average maximum strain d_{max} – were determined through isotropic line broadening analysis using simplified integral breadth methods for the (200) reflection of face-cantered cubic cells of Pt and Pd.

The chemical composition of the electrocatalytic coating surface was examined using X-ray photo-electron spectroscopy (XPS) on a Quantera II instrument (Physical Electronics, USA), which features a monochromatic X-ray source (AlK radiation, 1486 eV, 15 kV, 25 W). The analysis of the XPS peaks was carried out using the Peak Analyzer tool in OriginPro software (https://www.originlab.com). The peaks were fitted using Gaussian profiles by the least-squares method.

Semiconducting properties

Quasi-stationary voltammetry and electrochemical impedance spectroscopy were employed to investigate the electrochemical properties of the obtained materials, using a GAMRY Potentiostat/ /Galvanostat/ZRA Reference 3000 instrument. Voltammetry and EIS measurements were carried out in a standard temperature-controlled three-electrode cell. The platinum wire was the counter electrode. All potentials were measured and reported relative to the Ag/AgCl/KCl (saturated) reference electrode.

Thermal treatment of electrodes

It is known that palladium dissolves quite easily under anodic polarization [13-15]. Therefore, to mitigate palladium dissolution, the electrodes underwent thermal treatment in an air atmosphere. After thermal treatment at 500 °C, the surface of the samples acquired a characteristic blue color. The electrodes were thermally treated for 3 hours, although the surface took on a similar appearance after the first 15 minutes of treatment (Figure 1).

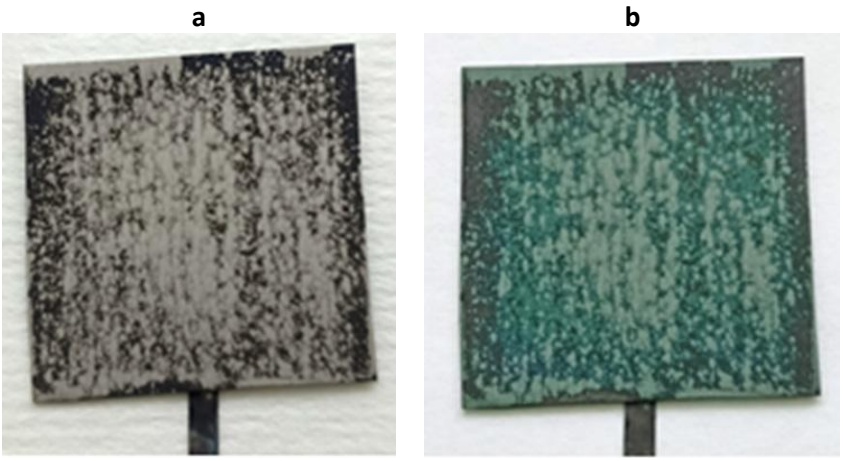

Figure 1. *Surface of the TiO_x-Pt-Pd electrode: (a) before and (b) after thermal treatment*

Electrocatalytic activity

The oxygen evolution reaction on the composite anodes was studied in 1 M $HClO_4$. The catalytic activity of the obtained anodes (4 cm^2) in sodium hypochlorite synthesis was assessed under electrolysis conditions in a 300 cm^3 solution of 0.9 g L^{-1} NaCl in a diaphragm-free cell with a titanium cathode at 25 °C. The anodic current density was 20 mA cm^{-2}. The salt solution was stirred using a compact electric stirrer. The current efficiency (CE, %) of NaClO was calculated by Equation (1):

$$CE_{NaClO} = \frac{2 \times 60 FVC_{NaClO}}{M_{NaClO} It} 100 \quad (1)$$

where C_{NaClO} / g L^{-1} is concentration of sodium hypochlorite in solution; t / min is the duration of electrolysis; V / L is electrolyte volume; F = 26.8 A h, M_{NaClO} = 74.5 g mol^{-1}, and I/A is electrolysis current.

Electrode lifetime assessment

The durability of the materials was assessed using an accelerated stability testing method, which involved electrolysis in a 1 M $HClO_4$ solution at a current density of 500 mA cm^{-2}, with continuous monitoring of the electrode potential over time. A sharp increase in potential was taken as an indication of electrode failure.

Results and discussion

The possibility of using microparticles of platinum group metals as catalysts on a titanium dioxide support was studied in works [16-18]. Systems with metals of the platinum group (Ru, Rh, Pd, Os, Ir, Pt) were investigated in the context of their adsorption capabilities in [16]. The growth of TiO_2 occurs through the movement of anions into vacant anion sites, as shown in the diagram (Figure 2). The rate of growth will depend on the number of defects in the crystalline lattice.

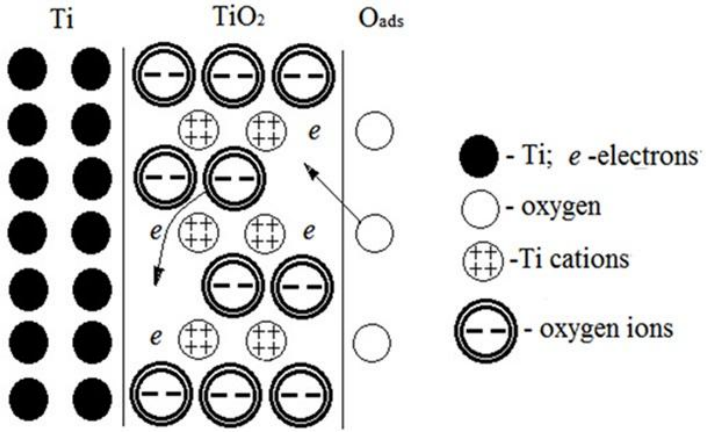

Figure 2. *Diagram of the formation of a TiO_2 film with vacant anion sites in the crystalline lattice*

There are noticeable trends toward the epitaxial growth of solid coatings on TiO_2 in the case of doping with noble metals. If the metal oxidizes upon contact with TiO_2, the substrate is also reduced to TiO_{2-x}. The environment significantly influences this process, especially the presence of oxygen, which can markedly alter the route of the reaction and the properties of the formed coatings [19,20].

There is a chemical engagement between the noble metal and TiO_2, as shown in work [21]. The authors explained this phenomenon by the local deficiency of anions on the substrate surface and, consequently, the interplay of metal atoms with the reduced cations of the substrate. For TiO_2, this effect directly correlates with the presence of Ti^{3+} ions on the surface and manifests as the migration of reduced titanium dioxide (TiO_{2-x}) [22] onto the surface of metallic particles, the spread of TiO_x

over the metal surface, and the movement of metal over the TiO_x surface, involving interactions between the metal and Ti from TiO_2 (primarily the Me-Ti^{3+} chemical bonding).

It was also established that some titanium is reduced and migrates into platinum clusters, which is one aspect of the interaction [23]. Moreover, encapsulation of platinum was observed [17,18], which is also noted in our work during the coating growth [11]. It is now generally accepted among the scientists that the noble metal particles become encapsulated by a thin suboxide (TiO_x) layer [24].

The formation of titanium suboxide contributes to the thermodynamic stability of the platinum coating on TiO_2; platinum atoms are predominantly adsorbed on titanium cations in fivefold coordination [23], which act as nucleation centres for platinum clusters. The authors did not find chemical bonds between stoichiometric TiO_2 and platinum; however, localized electron transfer occurs between Ti^{3+} and surface platinum atoms for pre-reduced TiO_2. Similar results (adsorption of platinum atoms on titanium cations in fivefold coordination, absence of interaction of platinum with the "ideal" TiO_2 surface, and charge transfer from Ti^{3+} to platinum) are reported in work [25].

Encapsulation of palladium particles at a temperature of 527 °C has also been reported [26]. Annealing in oxygen significantly affects materials containing palladium deposited on TiO_2 [27]: palladium nanoparticles on substoichiometric TiO_2 dissociatively adsorb oxygen at 400 °C, which "flows" onto the substrate, where onward reactions occur. The transferred oxygen re-oxidizes the surface, expelling embedded Ti^{n+} ions trapped in the crystal lattice, and promoting the re-growth of TiO_2 around and above the particles. This scheme was modelled in work [28] using a Monte Carlo model, and the results were confirmed by studies using scanning tunnelling microscopy. We assume that the growth of the coating in our work occurs similarly.

The morphology of the obtained materials was investigated using the SEM technique. The morphology of the coating without noble metals has been described in detail previously [11,29]. Overall, the morphology of mesoporous TiO_2 coatings doped with precious metals is characterized by a porous structure with uniformly distributed metal nanoparticles and a nanograined pattern.

Figure 3 presents SEM images of TiO_2 composites with a content of 0.5 mg cm^{-2} of Pt (Figure 3a), 0.5 mg cm^{-2} of Pd (Figure 3b), and 0.5 mg cm^{-2} of Pt and 0.5 mg cm^{-2} of Pd deposited sequentially (Figure 3c) after thermal treatment at 500 °C.

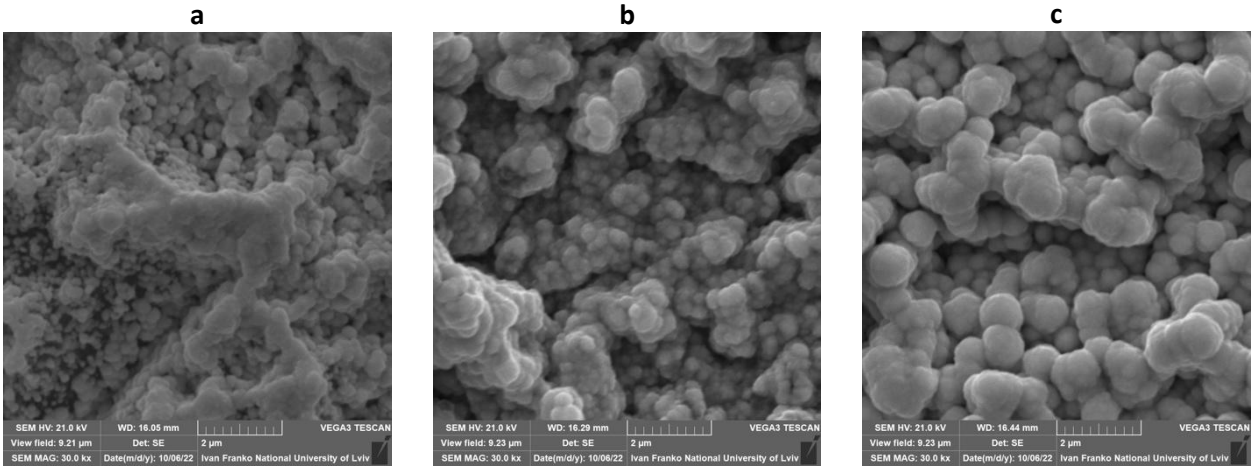

Figure 3. *SEM images of: (a) TiO_x-Pt, (b) TiO_x-Pd, (c) TiO_x-Pt-Pd*

The coatings have a well-developed surface, and their porosity is maintained even after the deposition of metal layers. The coatings are characterized by the presence of agglomerates or clusters, which are typical for composite materials obtained by deposition methods. According to energy-dispersive microanalysis (EDS) data, nearly all carbon was eliminated from the TiO_2 coating

following thermal treatment. A significant number of noble metals were found on the surface of the coatings (Figure 4).

The results obtained from the determination of the number of deposited metals using EDS and X-ray microanalysis methods differ. It is important to note that the EDS method does not reflect the metal content in the coating bulk. Microanalysis provided indirect evidence that platinum on the surface of the coating showed up in the metallic form, while palladium is determined in the form of an oxide. However, these assumptions require further confirmation.

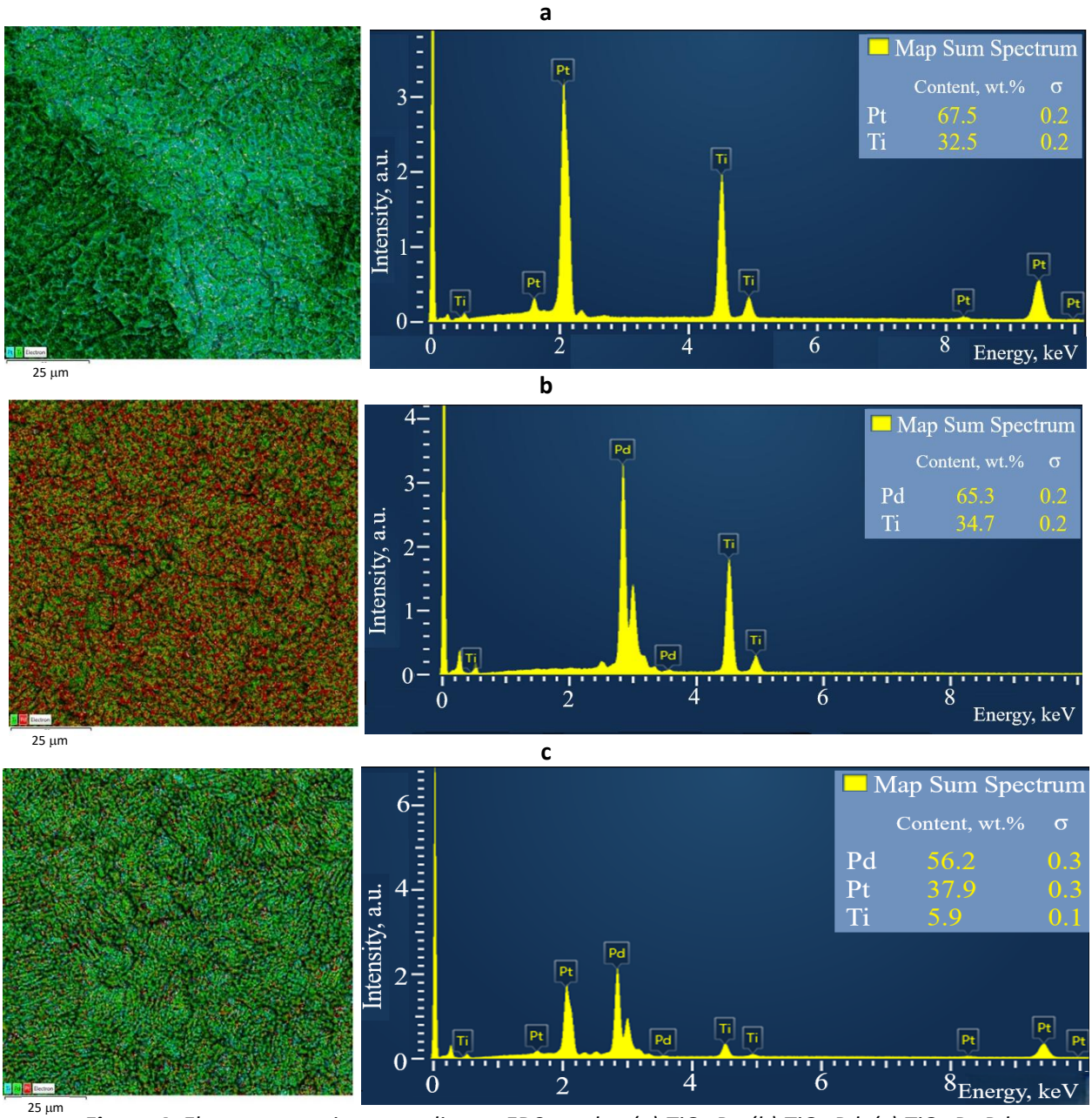

Figure 4. *Element mapping according to EDS results: (a) TiO_x-Pt, (b) TiO_x-Pd, (c) TiO_x-Pt-Pd*

Oxide coatings obtained by the electrochemical oxidation of titanium primarily exhibited an amorphous structure. Thermal treatment was carried out at temperatures above 300 °C to achieve the crystalline structure necessary for practical applications. X-ray diffraction patterns of the TiO_x-Pt, TiO_x-Pd, and TiO_x-Pt-Pd samples after thermal treatment at 500 °C are shown in Figure 5.

The phase composition of the coating was determined by the characteristic diffraction peaks of anatase TiO_2 observed at 2θ = 25.2, 36.7, 37.5, 38.7, 47.8, 53.6, 55, 62.6, 68.8, 70.4 and 75.1°.

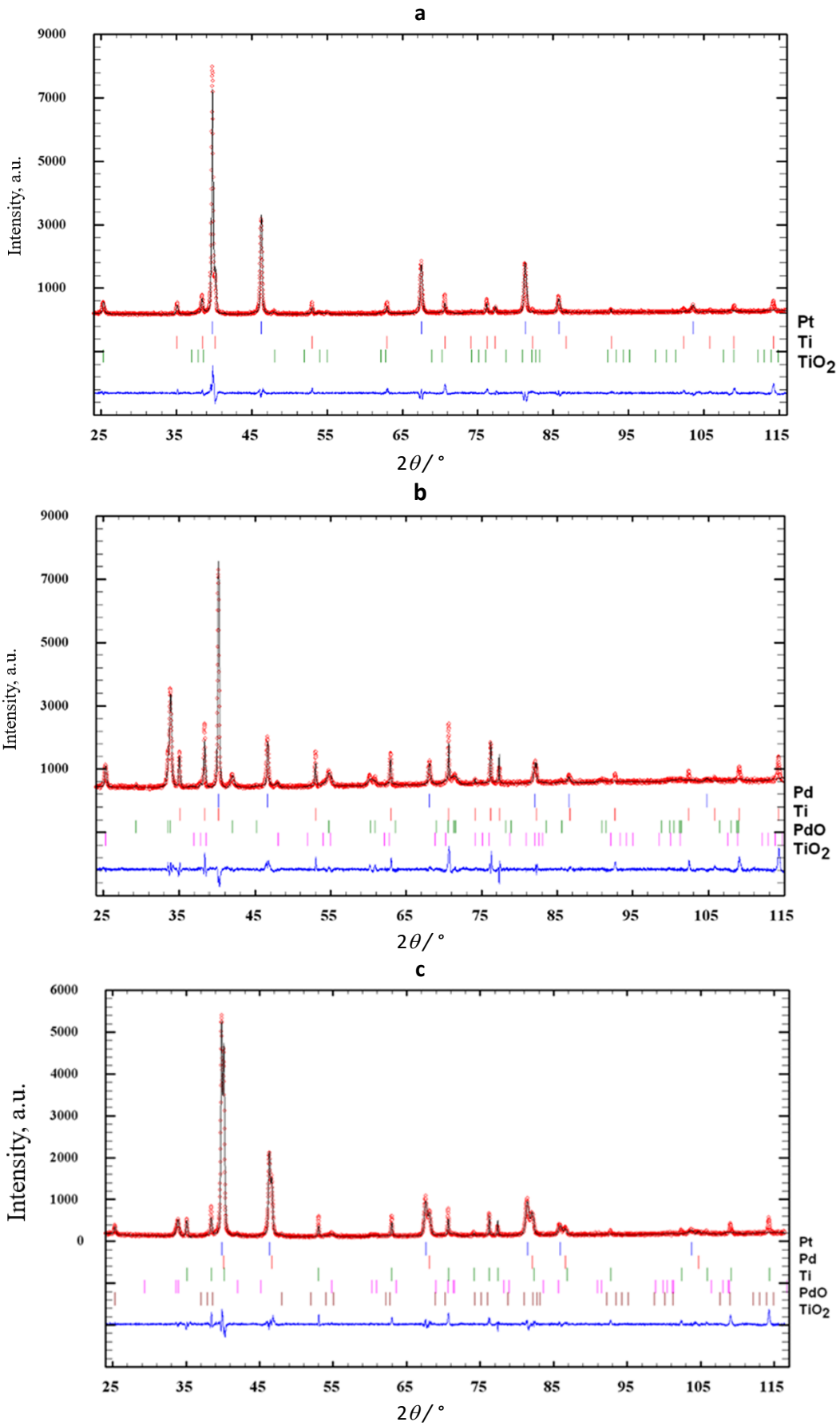

Figure 5. *Observed and calculated X-ray powder profiles for: (a) TiO_x-Pt, (b) TiO_x-Pd, (c) TiO_x-Pt-Pd. Experimental data (circles) and calculated profile (solid line through the circles) are presented together with the calculated Bragg positions (vertical ticks) and difference curve (bottom solid line)*

These peaks correspond to the (101), (103), (004), (112), (200), (105), (211), (204), (116), (220) and (215) crystallographic planes of the anatase phase; for metallic Ti at 2θ = 34.95, 38.25, 40.05 and 52.90°; for Pt at 2θ = 39.8, 46.2 and 67.5°; for Pd at 2θ = 40.1, 46.6 and 68.1°; and for PdO at 2θ = 33.56, 33.89 and 41.95° [30,31].

In the case of the Pt-loaded series, no additional peaks were observed, neither from other crystallographic forms of TiO_2, nor from Pt nanoparticles. However, for the Pt-containing sample, a diffraction peak at 2θ = 40.1° was detected, corresponding to the (111) plane of metallic platinum, confirming its presence in the sample [32]. Crystal structures of the phases were refined by the Rietveld method with the program FullProf.2k, applying a pseudo-Voigt profile function and isotropic approximation for the atomic displacement parameters. Phase composition of the investigated samples, crystallographic data and microstructural parameters for the phases with face-centered cubic (fcc) structure (structure type Cu, space group *Fm*–3*m*) are summarized in Table 1. Microstructural parameters (*i.e*. size of coherently diffracting domains accepted as average apparent crystallite size *D*, and average maximum strain (d_{max})) were identified by isotropic line broadening analysis using simplified integral breadth methods for (200) reflection of face-centered cubic cells of Pt and Pd. Almost all refined structural, profile, and instrumental parameters enter the profile function formula nonlinearly. The methods for estimating nonlinear parameters represent an iterative process, where at each iteration the so-called increments (shifts) are determined using the least squares method. The new value of each refined parameter is calculated as the sum of its value from the previous iteration and its increment from the current iteration. At each iteration, a covariance matrix is calculated to determine the variances of the increments, which are also the variances of the refined parameters.

Table 1. *The phases and chemical composition of experimental materials, crystallographic data and microstructural parameters for phases with a face-centered cubic (fcc) structure. The square root of the variance (standard deviation) is shown in parentheses next to the parameter values*

Sample	Phase contribution[1], wt.%	*a* / nm*	Unit cell volume, nm^3	*D* / nm	d_{max}
0.5 mg cm^{-2} Pt	Pt 46.2(4) Ti [2] 38.5(7) TiO_2 ana[3] 15.3(5)	0.392146(9)	0.060304(2)	27.1	0.0036
0.5 mg cm^{-2} Pd	Pd 22.8(4) Ti 43.2(6) TiO_2 ana 12.9(4) PdO[4] 21.1(3)	0.389124(13)	0.058920(3)	25.2	0.0038
0.5 mg cm^{-2} Pt 0.5 mg cm^{-2} Pd	Pt 42.8(5) Pd 19.5(3) Ti 28.4(4) TiO_2 ana 5.2(2) PdO 4.1(1)	0.391689(14) 0.389132(16)	0.060093(4) 0.058924(4)	24.3 23.1	0.0040 0.0042

[1]The quantitative phase contribution refers to the sample's surface; [2]Ti has a structure type like Mg, with a space group of $P6_3/mmc$; [3]TiO_2 anatase has a space group of $I4_1/amd$; [4]PdO room-temperature modification (pallandite) has a structure type like PtS, with a space group of $P4_2/mmc$; *lattice parameter

The presence of Pt diffraction peaks in the diffraction pattern indicates the effective deposition of nanocrystalline Pt particles on the material's surface, likely organized into clusters large enough to produce characteristic diffraction signals of appreciable intensity. Notably, in the analysed series, no shifts in the TiO_2 pattern peaks were observed upon Pt loading. This suggests that Pt is not incorporated into the TiO_2 lattice but is deposited onto the surface of the oxide. Similar results were obtained in the work [33].

Titanium dioxide without thermal treatment often exhibits an X-ray amorphous structure. This is because the material lacks an ordered crystalline structure that would yield characteristic diffraction peaks. Thermal treatment enables the production of materials with a crystalline structure. Similar results have been obtained previously [34].

During the thermal treatment of samples at 500 °C for 3 hours, a growth in the fraction of the crystal phase was observed. The main crystal phase is anatase of titanium dioxide. Metallic titanium is present on the surface in amounts less than 1 wt.%. In the samples, palladium is found in both metallic and oxide forms, while platinum is present in metallic form in all samples.

Moreover, to elucidate the chemical composition and the surface electronic state of Pd, X-ray photoelectron spectroscopic (XPS) analyses were conducted. The total survey spectrum confirms the high purity of the catalysts and reveals the coexistence of Ti, Pt, and Pd in the samples.

In the XPS spectra of the TiO_2 surface coated with a layer of metals, distinct signals corresponding to Ti 2p, O 1s, Pt 4f, and Pd 3d are observed. The Ti 2p signal with binding energies of Ti $2p_{3/2}$ (458.8 eV) and Ti $2p_{1/2}$ (464.4 eV), corresponding to titanium in the +4 oxidation state, is observed [35] (Figure 6a), which is consistent with literature results [36,37]. The absence of any shift in the energy of the Ti 2p peaks confirms that the incorporation of platinum is limited to surface modification, with no integration of Pt into the TiO_2 lattice structure.

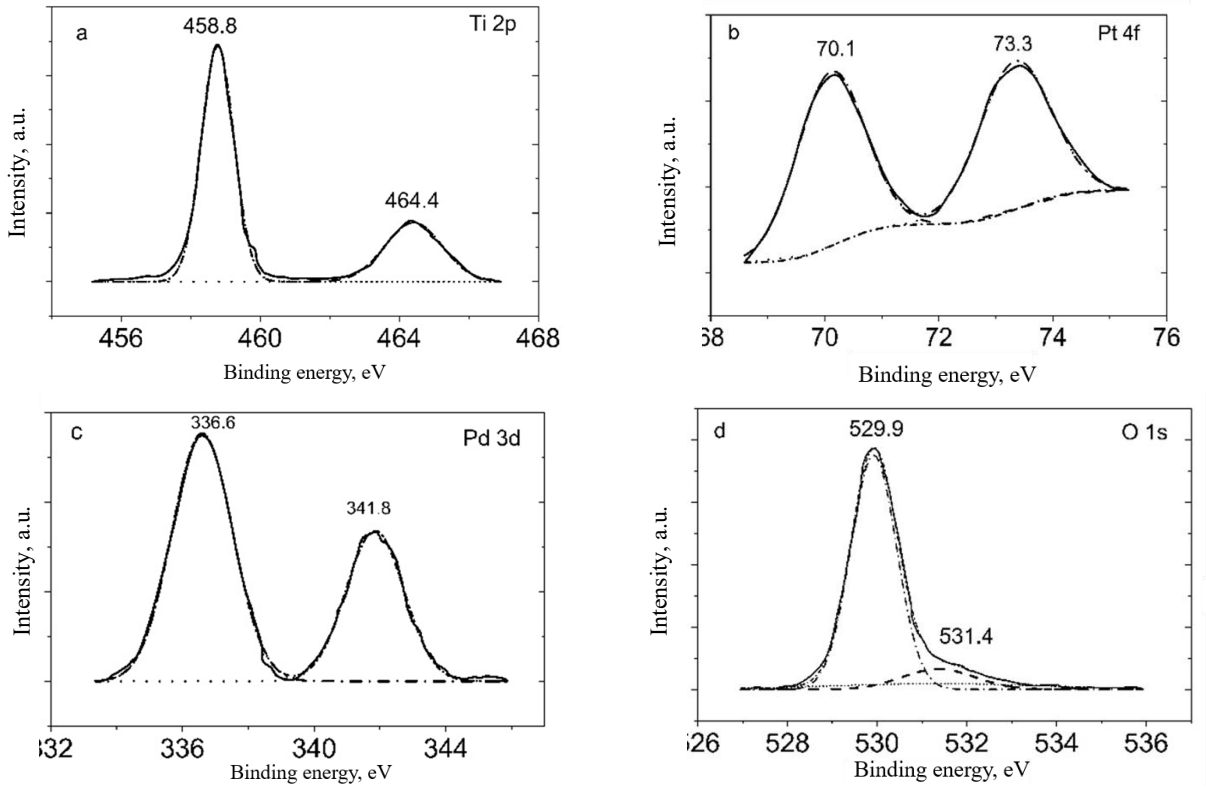

Figure 6. *Simulated XPS spectra of (a) Ti 2p, (b) Pt 4f, (c) Pd 3d, (d) O 1s core level structures in TiO_2-Pt-Pd composites*

The O 1s peak (531 eV) contains two maxima at 529.9 and 531.4 eV (Figure 6d). Its binding energy is too high for metal oxide-hydroxide compounds and instead is characteristic of oxygen in adsorbed water molecules [35,38]. Most likely, the first peak corresponds to oxygen in the TiO_2 compound, while the second corresponds to OH^- ions that compensate for the excess charge of cation vacancies and the outer layers of water [39]. The oxygen peak at 529.9 eV indicates the predominance of strongly bound oxygen at the surface of the TiO_2 crystalline lattice. The intensity of the inert oxygen-

containing particle peak is significantly lower for the metal-coated samples compared to weakly bound species. The Pt 4f region spectrum was analysed and fitted with a doublet (Figure 6b), with a separation of 3.2 eV between the $f_{7/2}$ and $f_{5/2}$ peaks [33]. The mainline $4f_{7/2}$ peak was observed at a binding energy of 70.1 eV, indicating the presence of metallic platinum on the surface [40]. The palladium spectrum shows two maxima at 341.8 and 336.6 eV (Figure 6c), which are attributed to the spin-orbit splitting of Pd $3d_{5/2}$ and Pd $3d_{3/2}$ of Pd^{2+} [41]. These binding energy values differ from those (340.1 and 334.9 eV) for metallic Pd [42], which also indirectly indicates that palladium in the samples is in the form of PdO and is consistent with the results from X-ray diffraction and microanalysis.

The photocatalytic performance of a semiconductor photocatalyst is significantly influenced by the alignment of its electronic energy levels, particularly the flat band potential. The energy band positions were determined using Mott–Schottky analysis. The Mott–Schottky plot depicts the relationship between the inverse square of the apparent capacitance ($1/C^2$) and the applied potential within the depletion region of a semiconductor–electrolyte junction. This analysis provides critical insights into the semiconductor's electronic properties, such as carrier concentration and flat band potential, which are essential for understanding its photocatalytic behaviour, Equation (2):

$$E_{fb} = E_{C^{-2}=0} + \frac{e\varepsilon\varepsilon_0 N}{2C_H^{\ 2}} - \frac{kT}{e} \quad (2)$$

where C_H is the Helmholtz layer capacitance in the semiconductor, e is the elementary charge, ε is the dielectric constant of the semiconductor, ε_0 is the permittivity of free space, N is the carrier density, E is the applied potential, E_{fb} is the flat band potential, k is the Boltzmann constant, and T is the absolute temperature.

The flat band potential (E_{fb}) is determined by extrapolating the linear region of the Mott-Schottky plot, while the slope is linked to the semiconductor's carrier density. The Mott-Schottky plots of the TiOx-based samples exhibited a positive slope, confirming their n-type semiconductor behaviour (Figure 7); thus, the E_{fb} values relate to the conduction band potential.

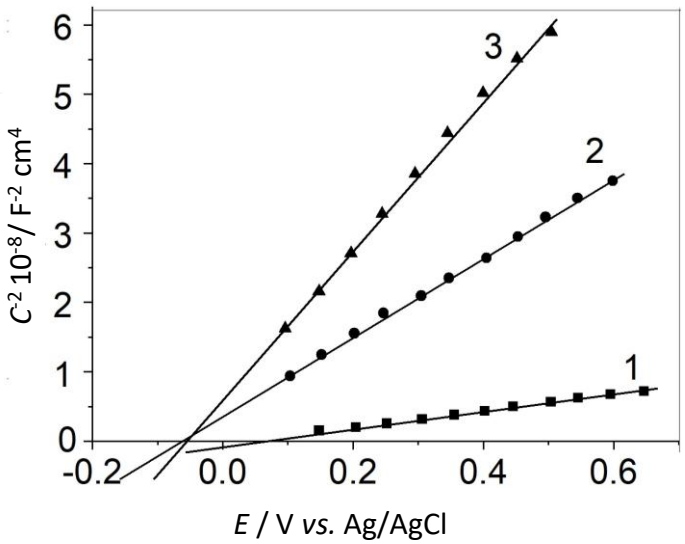

Figure 7. *Mott–Schottky plots for: (1) TiO_x-Pt, (2) TiO_x-Pd, (3) TiO_x-Pt-Pd, solution: 1 M $HClO_4$, frequency: 1000 Hz*

The E_{fb} values were found to be 0.03, -0.07 and -0.05 V for TiO_x-Pt, TiO_x-Pd, and TiO_x-Pt-Pd, respectively. The electron densities for TiO_x-Pt, TiO_x-Pd, and TiO_x-Pt-Pd were 2.99×10^{22}, 6.23×10^{21}, and 3.27×10^{21} cm^{-3}, respectively (Table 2). The slope b in Table 2 is related to semiconductor material parameters such as band gap and electron mobility.

Doping of TiO_2 with Pt and Pd resulted in a negative shift of the conduction band and an increase in the dopant density due to the electrocatalytic effect of platinum and improved electron transfer [43].

Table 2. *Semiconductor properties of titanium suboxide-based composites*

Sample	Slope × 10^{-8}, F^{-2} cm^4 V^{-1}	Carriers' density×10^{-21}, cm^{-3}	E_{fb} / V
TiO_x-Pt	1.18	29.9	0.032
TiO_x-Pd	5.67	6.23	-0.07
TiO_x-Pt-Pd	10.8	3.27	-0.05

The obtained materials are highly doped n-type semiconductors [29,44].

Electrodes containing Pt exhibit a higher flat band potential compared to those with Pd. This observed effect can be attributed to the fact that in electrodes with a high content of platinum, the amount on the surface does not change during thermal treatment. Thus, the reduction in the number of carriers leads to an increase in the impact of the semiconductor component, resulting in a steepening of the polarization curves for TiO_x-Pt-Pd (see Figure 7).

The electrocatalytic activity of the obtained materials was studied for the oxygen evolution reaction (OER). The complexity of the four-electron (OER arises from its multistep mechanism and the involvement of adsorbed oxygen species on the electrode surface. According to Trasatti [45 and references herein], Ferster was the first to suggest that oxygen evolves through the decomposition of unstable intermediate oxides. The transition of these intermediates into stable oxides or back to the metal with oxygen gas release defines the reaction kinetics.

Numerous kinetic schemes have since been proposed [45], most starting with the formation of adsorbed OH or O species *via* water or OH^- discharge:

$$H_2O \leftrightarrow OH_{ads} \leftrightarrow O_{ads} \quad (3)$$

Subsequent transformations may include chemical or electrochemical desorption steps:

$$2O_{ads} \leftrightarrow O_2 \quad (4)$$

$$O_{ads} + H_2O \leftrightarrow O_2 + 2H^+ + 2e^- \quad (5)$$

$$2[O_{ads} + MO_x \leftrightarrow MO_{x+1}] \leftrightarrow O_2 + 2MO_x \quad (6)$$

(M – electrode material)

The overpotential typically arises from the inhibition of one or more of these steps. At moderate current densities, the rate is likely limited by the formation of adsorbed oxygen species, explaining the observed Tafel slope of $b \approx 0.12$ V dec^{-1}. Under other conditions, later stages or a sequence of steps may become rate-determining [45]. Tafel plot "kinks" at higher overpotentials can result from: i) a mechanism shift, ii) a change in the rate-limiting step, or iii) varying surface coverage [45].

The oxygen evolution overpotential on the TiO_x-Pt-Pd material was lower than that of the platinized electrode and significantly lower than the palladium-only electrode (Figure 8). The Tafel slope decreases as the noble metal content in the composite increases. For the oxide that contains 0.5 mg cm^{-2} of Pt and 0.5 mg cm^{-2} of Pd (curve 3), it is 92 mV dec^{-1}, while for electrodes with 0.5 mg cm^{-2} of Pt (curve 1) and 0.5 mg cm^{-2} of Pd (curve 2), it is 111 and 55 mV dec^{-1}, respectively. Such a minor deviation from the theoretical value for the TiO_x-Pt-Pd sample can be understood by the inhomogeneity of the composite or the advanced surface of the coating. In the case of a significant deviation, more than twice for the TiO_x-Pd sample, it may be explained by a change in the rate-limiting step of the oxygen evolution reaction [45]. It is likely that in the case of palladium-modified coatings, the rate-limiting step is the so-called electrochemical desorption, indirectly evidenced by the area of the peak corresponding to labile oxygen-containing species in the O1s region of the X-ray photoelectron spectrum.

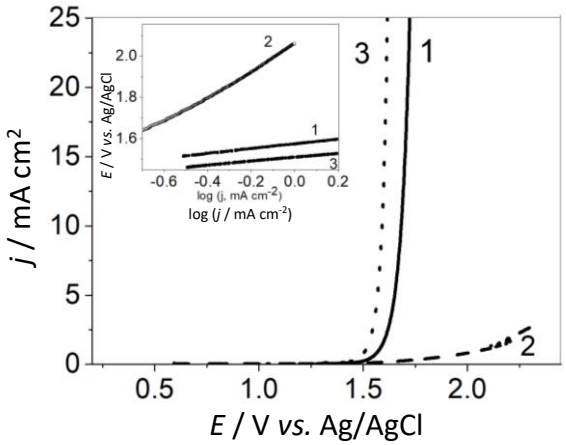

Figure 8. *Quasi-stationary polarization curves for oxygen evolution in 1 M $HClO_4$ for: (1) TiO_x-Pt, (2) TiO_x-Pd, (3) TiO_x-Pt-Pd. Inset: curves represented in semilogarithmic scale*

In Figure 9, the reproducible polarization curves for the TiO_x-Pt-Pd anode and the thermally treated TiO_x-Pt-Pd-500 °C in 1 M $HClO_4$ are presented. The thermally treated anode exhibits a reduction in polarization of 150 mV. In each case, the *E-log j* curves demonstrate a linear relationship (Figure 9b). The Tafel slope for the untreated sample is 160 mV dec^{-1}, while for the thermally treated electrode, it is 92 mV dec^{-1}.

Thus, during thermal treatment, there is a noticeable decrease in the slope of the Tafel equation (*b*). This may suggest that the surface becomes more homogeneous, facilitating the desorption of oxygen or altering the mechanism, resulting in an increased rate of the first electron transfer [46].

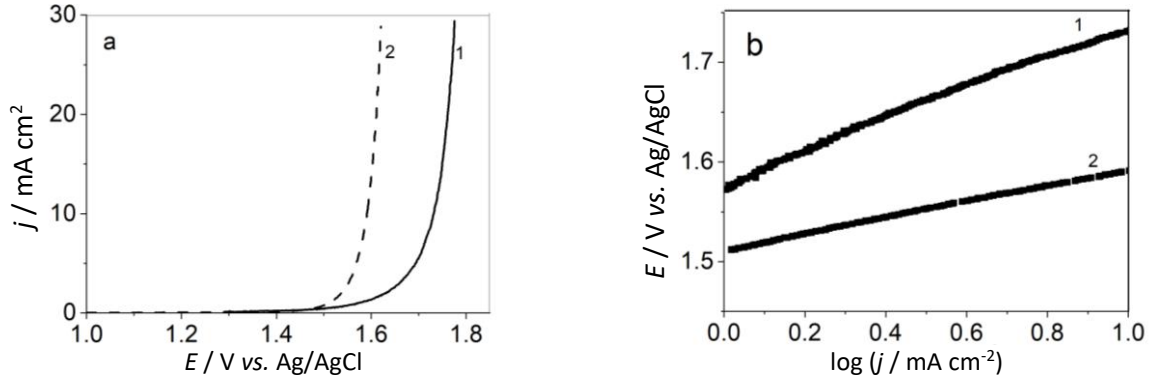

Figure 9. *(a) Quasi-stationary polarization curves for oxygen evolution in 1 M $HClO_4$, (b) curves represented in semilogarithmic scale for TiO_x-Pt-Pd: (1) untreated, (2) thermally treated at 500 °C during 3 h. Potential scan rate 5 mV s^{-1}*

The role of temperature and processing time on the oxygen evolution reaction for a coating containing sequentially deposited layers of platinum and palladium was also investigated (Figure 10). It is known that at temperatures above 600 °C, titanium nitrides [47] are formed, which is undesirable. Moreover, with an increase in temperature, the mechanical properties of titanium deteriorate [48]. Therefore, the temperature range was selected to obtain composite coatings with the desired phase composition.

The obtained results show that at a temperature of 500 °C, the oxygen evolution overpotential is the lowest. This extreme dependence is most likely associated with the different growth rates of TiO_2 depending on the temperature. As the temperature rises to 500 °C, the fraction of the crystalline phase increases. During thermal treatment, metals on the surface migrate more uniformly into the bulk during coating growth. This leads to a more even redistribution of current density and, as a result, a reduction in overpotential.

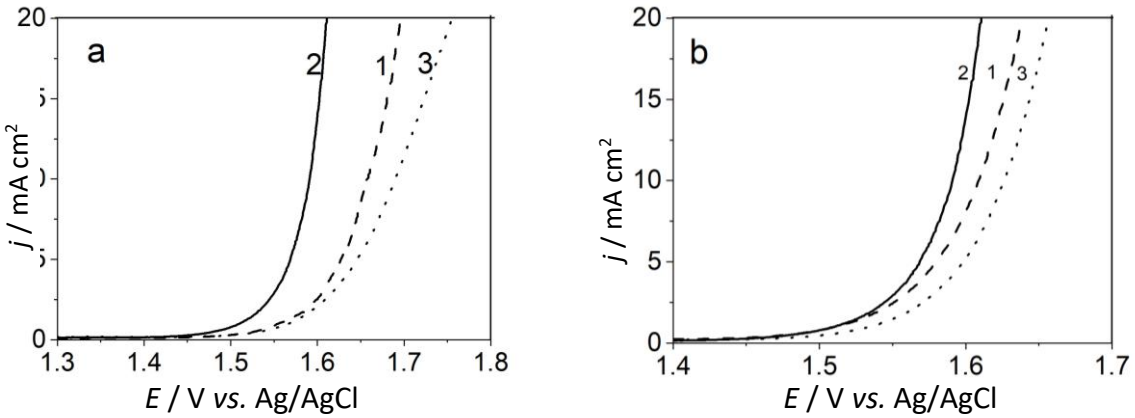

Figure 10. *(a) Quasi-stationary polarization curves for oxygen evolution in 1 M $HClO_4$ for TiO_x-Pt-Pd thermally treated at the following temperatures: (1) 400; (2) 500; (3) 600 °C. (b) Curves for TiO_x-Pt-Pd thermally treated at 500 °C during the following times: (1) 1; (2) 3; (3) 6 hours. Potential scan rate 5 mV s^{-1}*

Further temperature increases above 600 °C may lead to the loss of titanium strength. The thermal treatment time also shows an extreme dependence. As seen from the graph, the dependence passes through a minimum, so the optimal thermal treatment time was chosen to be 3 hours.

It is known that coatings with a layer of metallic palladium, thermally treated at temperatures of 500-530 °C, can be an effective anode for the synthesis of hypochlorous acid from low-concentration NaCl solutions [49,50]. We investigated the electrocatalytic activity of several materials, including those traditionally used in the synthesis of hypochlorous acid. Results are shown in Table 3. The thermally treated TiO_x-Pt-Pd anode with a surface noble metal content of 0.5 mg cm^{-2} demonstrated the highest catalytic properties and selectivity for the hypochlorite synthesis reaction among the studied samples. The CE for NaClO production at a current density of 40 mA cm^2 was 90 %.

Table 3. *Comparison of current efficiency (CE) of HClO synthesis from low-concentration Cl-containing solutions for various materials*

Material	CE of HClO synthesis, %
Ti/Pt	37
SnO_2-Sb	89
Ti/IrO_x	80
Ti/RuO_x-IrO_x	70
TiO_x-Pt	89
TiO_x-Pd	86
TiO_x-Pt-Pd	90

We also studied the corrosion resistance of the materials using an accelerated stability assessment method, which involved electrolysis in a 1 M $HClO_4$ solution at a current density of 500 mA cm^{-2} while recording the electrode potential over time. The electrode was considered failed if a sharp potential jump occurred. The lifetime of the coating with sequentially deposited layers of platinum and palladium was 176 hours, which exceeded the lifetime of the coating containing only platinum. The electrode coated only with a layer of palladium was unstable and degraded quickly.

Unlike many nanoparticle-stabilized systems, which rely heavily on colloidal or sol-gel synthesis and often suffer from agglomeration or loss of activity over time, this work presents a structurally robust, porous, and thermally stable coating. Moreover, it demonstrates superior stability (176 h at 500 mA cm^{-2}) and exceptional selectivity in hypochlorite production (90 % efficiency), which are rarely achieved simultaneously in similar systems. The method also provides scalable and cost-

effective fabrication pathways suitable for industrial applications, particularly in electrochemical oxidation and cathodic protection.

Conclusion

It has been established that titanium suboxide-based composites with low noble metal content have a developed porous surface, which remains intact even after the deposition of metal layers. The main allotrope form of TiO_x in the studied composite materials is anatase, along with metallic titanium, platinum, palladium, and palladium oxide. Platinum is present in its metallic form, while palladium exists both as a metal and oxide, which is consistent with the results of X-ray photo-electron spectroscopy and X-ray diffraction. Electrochemical studies using the Mott-Schottky method showed that the composites exhibit n-type conductivity with a high concentration of charge carriers. The oxygen evolution overpotential on the material containing platinum and palladium is lower than that of the platinized coating, and significantly lower than that of the electrode containing only palladium. In summary, the thermally treated TiO_x-Pt-Pd anode exhibits superior catalytic performance and durability, with a NaClO production efficiency of 90 % and a lifetime exceeding 176 hours at 500 mA cm^{-2}. These findings suggest its potential for practical electro-chemical applications.

Author contributions: *Conceptualization: [Olesia Shmychkova]; Methodology: [Tatiana Luk'yanenko]; Formal analysis and investigation: [Valentina Knysh; Heorhii Zhemela]; Writing - original draft preparation: [Olesia Shmychkova]; Writing - review and editing: [Alexander Velichenko]; Funding acquisition: [Alexander Velichenko]; Resources: [Alexander Velichenko]; Supervision: [Alexander Velichenko].*

Funding: *This work was supported by the Ministry of Education and Science of Ukraine [grant number 0123U101809].*

Data availability: *Data will be made available by the corresponding author on reasonable request.*

Conflict of interest: *All authors certify that they have no affiliations with or involvement in any organization or entity with any financial interest or non-financial interest in the subject matter or materials discussed in this manuscript.*

References

[1] J. Zhao, H. Wang, Ya. Cai, J. Zhao, Z. Gao, Ya.-Ya. Song, The challenges and opportunities for TiO_2 nanostructures in gas sensing, *ACS Sensors* **9** (2024) 1644-1655. https://doi.org/10.1021/acssensors.4c00137

[2] A. Garzon-Roman, C. Zuñiga-Islas, D. H. Cuate-Gomez, A. Heredia-Jimenez, TiO_2/porous silicon heterostructures formation by simple and low-cost methods for electronics applications, *Sensors and Actuators A* **349** (2023) 114064. https://doi.org/10.1016/j.sna.2022.114064

[3] C. P. Ferraz, S. Navarro-Jaen, L. M. Rossi, F. Dumeignil, M. N. Ghazzal, R. Wojcieszak, Enhancing the activity of gold supported catalysts by oxide coating: Towards efficient oxidations, *Green Chemistry* **23** (2021) 8453-8457. https://doi.org/10.1039/D1GC02889H

[4] F. Riboni, N.T. Nguyen, S. So, P. Schmuki, Aligned metal oxide nanotube arrays: key-aspects of anodic TiO_2 nanotube formation and properties, *Nanoscale Horizons* **1** (2016) 445-466. https://doi.org/10.1039/C6NH00054A

[5] S. Harada, K. Tanaka, H. Inui, Thermoelectric properties and crystallographic shear structures in titanium oxides of the Magneli phases, *Journal of Applied Physics* **108** (2010) 083703. https://doi.org/10.1063/1.3498801

[6] X. Chang, S. S. Thind, A. Chen, Electrocatalytic enhancement of salicylic acid oxidation at electrochemically reduced TiO_2 nanotubes, *ACS Catalysis* **4** (2014) 2616-2622. https://doi.org/10.1021/cs500487a

[7] N. J. Suliali, C. M. Mbulanga, W. E. Goosen, R. Botha, Current density transient response to variations in synthesis parameters during anodic growth of TiO_2 nanotubes, *Materials Science in Semiconductor Processing* **109** (2020) 104931. https://doi.org/10.1016/j.mssp.2020.104931
[8] O. Kasian, T. Luk'yanenko, A. Velichenko, Oxidation of Cr^{3+} ions at the composite TiO_x/PtO_y electrode, *ECS Transactions* **45** (2013) 13-18. https://doi.org/10.1149/04509.0013ecst
[9] O. I. Kasian, T. V. Luk'yanenko, A. B. Velichenko, Electrochemical properties of heat treated platinized titanium, *Protection of Metals and Physical Chemisty of Surfaces* **49** (2013) 559-566. https://doi.org/10.1134/S2070205113050043
[10] C. C. Hu, C. H. Lee, T. C. Wen, Oxygen evolution and hypochlorite production on Ru Pt binary oxides, *Journal of Applied Electrochemistry* **26** (1996) 72-82. https://doi.org/10.1007/BF00248191
[11] A. Velichenko, V. Kordan, O. Shmychkova, V. Knysh, P. Demchenko, The effect of Ti/TiO_2 treatment on morphology, phase composition and semiconductor properties, *Voprosy Khimii i Khimicheskoi Tekhnologii* **4** (2022) 18-23. https://doi.org/10.32434/0321-4095-2022-143-4-18-23
[12] O. B. Shmychkova, T. V. Luk'yanenko, R. Amadelli, A. B. Velichenko, PbO_2 anodes modified by cerium ions, *Protection of Metals and Physical Chemistry of Surfaces* **50** (2014) 493-498. https://doi.org/10.1134/S2070205114040169
[13] J. Genesca, R. Duran, The effect of Cl^- on the kinetics of the anodic dissolution of Pd in H_2SO_4 solutions, *Electrochimica Acta* **32** (1987) 541-544. https://doi.org/10.1016/0013-4686(87)87039-1
[14] J. Genesch, The electrodissolution kinetics of palladium. A note on the effect of chloride ion concentration, *Platinum Metals Review* **30** (1986) 80-83. https://doi.org/10.1595/003214086X3028083
[15] A. D. Styrkas, D. A. Styrkas, Purification of palladium by AC electrodissolution and electrodeposition, *Inorganic Materials* **36** (2000) 1114-1117. https://doi.org/10.1007/BF02758927
[16] S.J. Tauster, S.C. Fung, R.L Garten, Strong metal-support interactions. Group 8 noble metals supported on TiO_2, *Journal of the American Chemical Society* **100** (1978) 171-175. https://doi.org/10.1021/ja00469a029
[17] O. Dulub, W. Hebenstreit, U. Diebold, Imaging cluster surfaces with atomic resolution: the strong metal-support interaction state of Pt supported on TiO_2 (110), *Physical Review Letters* **84** (2000) 3646-3649. https://doi.org/10.1103/PhysRevLett.84.3646
[18] F. Pesty, H.-P. Steinriick, T. E. Madey, Thermal stability of Pt films on TiO_2(110): evidence for encapsulation, *Surface Science* **339** (1995) 83-95. https://doi.org/10.1016/0039-6028(95)00605-2
[19] H. Park, Yi. Park, W. Kim, W. Choi, Surface modification of TiO_2 photocatalyst for environmental applications, *Journal of Photochemistry and Photobiology C: Photochemistry Reviews* **15** (2013) 1-20. https://doi.org/10.1016/j.jphotochemrev.2012.10.001
[20] C. L. Munich, Yu. Zhou, A. M. Holder, A. Weimer, Ch. B. Musgrave, Effect of surface deposited Pt on the photoactivity of TiO_2, *The Journal of Physical Chemistry C* **116** (2012) 10138-10149. https://doi.org/10.1021/jp301862m
[21] S. J. Tauster, Strong metal-support interactions, *Accounts of Chemical Research Journal* **20** (1987) 389-394. https://doi.org/10.1021/ar00143a001
[22] A. K. Datye, D. S. Kalakkad, M. H. Yao, D. J. Smith, Comparison of metal-support interactions in Pt/TiO_2 and Pt/CeO_2, *Journal of Catalysis* **155** (1995) 148-153. https://doi.org/10.1006/jcat.1995.1196
[23] K. D. Schierbaum, S. Fischer, M. C. Torquemada, J. L. de Segovia, E. Roman, J. A. Martin-Gago, The interaction of Pt with TiO_2 (110) surfaces: a comparative XPS, UPS, ISS, and ESD study, *Surface Science* **345** (1996) 261-273. https://doi.org/10.1016/0039-6028(95)00887-X

[24] F. Kraushofer, M. Krinninger, S. Kaiser, J. Reich, A. Jarosz, M. Fuchsl, G. Anand, F. Esch, B.A.J. Lechner The influence of bulk stoichiometry on near-ambient pressure reactivity of bare and Pt-loaded rutile TiO_2(110), *Nanoscale* **16** (2024) 17825-17837. https://doi.org/10.1039/D4NR01702A
[25] S. Fischer, K. D. Schierbaum, W. Gopel, Surface defects and platinum overlayers on TiO_2 (110) surfaces: STM and photoemission studies, *Vacuum* **48** (1997) 601-605. https://doi.org/10.1016/S0042-207X(97)00045-6
[26] Z. Chang, G. Thornton, Effect of Pd on the interaction of formic acid with TiO_2 (110), *Surface Science* **459** (2000) 303-309. https://doi.org/10.1016/S0039-6028(00)00458-1
[27] R. A. Bennett, P. Stone, M. Bowker, Pd nanoparticle enhanced re-oxidation of non-stoichiometric TiO_2: STM imaging of spillover and a new form of SMSI, *Catalysis Letters* **59** (1999) 99-105. https://doi.org/10.1023/A:1019053512230
[28] A. J. Ramirez-Cuesta, R. A. Bennett, P. Stone, P. C. H. Mitchell, M. Bowker, STM investigation and Monte-Carlo modelling of spillover in a supported metal catalyst, *Journal of Molecular Catalysis A: Chemical* **167** (2001) 171-179. https://doi.org/10.1016/S1381-1169(00)00504-5
[29] O. Shmychkova, V. Knysh, T. Luk'yanenko, A. Velichenko, Physicochemical and electrochemical properties of materials based on titanium suboxides, *Surface Engineering and Applied Electrochemistry* **60** (2024) 232-240. https://doi.org/10.3103/S106837552402011X
[30] L. Messaadia, S. Kiamouche, H. Lahmar, R. Masmoudi, H. Boulahbel, M. Trari, M. Benamira, Solar photodegradation of Rhodamine B dye by Cu_2O/TiO_2 heterostructure: experimental and computational studies of degradation and toxicity, *Journal of Molecular Modeling* **29** (2023) 38. https://doi.org/10.1007/s00894-023-05449-z
[31] A. Crespo, J. Gallenberger, M. De Santis, V. Langlais, F. Carla, J.M. Caicedo, J. Rius, X. Torrelles, Heteroepitaxial growth of anatase (001) films on $SrTiO_3$ (001) by PLD and MBE, *Applied Surface Science* **632** (2023) 157586. http://doi.org/10.2139/ssrn.4282778
[32] H. Wang, R. Yao, R. Zhang, H. Ma, J. Gao, M. Liang, Y. Zhao, Z. Miao, CeO_2-supported TiO_2–Pt nanorod composites as efficient catalysts for CO oxidation, *Molecules* **28** (2023) 1867. https://doi.org/10.3390/molecules28041867
[33] A. Kubiak, T. Rozmanowski, E. Gabala, P. Krawczyk, Comprehensive spectroscopy and photocatalytic activity analysis of TiO_2-Pt systems under LED irradiation, *Scientific Reports* **14** (2024) 13827. https://doi.org/10.1038/s41598-024-64748-4
[34] I. M. Gavrilin, A. A. Dronov, Yu. I. Shilyaeva, E. A. Lebedev, M. S. Kuzmicheva, T. P. Savchuk, S. A. Gavrilov, Improved photoanode structure based on anodic titania nanotube array covered by TiO_2-NPs/nanographite composite layer for ETA-cells, *Journal of Physics: Conference Series* **741** (2016) 012100. https://doi.org/10.1088/1742-6596/741/1/012100
[35] D. Briggs, M.P. Seah (Eds.), *Practical Surface Analysis in Auger and X-Ray Photoelectron Spectroscopy*, John Wiley & Sons, Chichester, England, 1990, p. 674. ISBN 0-471-92081-9.
[36] M. C. Biesinger, B. P. Payne, A. P. Grosvenor, L. W. M. Lau, A. R. Gerson, R. St. C. Smart, Resolving surface chemical states in XPS analysis of first row transition metals, oxides and hydroxides: Cr, Mn, Fe, Co and Ni, *Applied Surface Science* **257** (2011) 2717-2730. https://doi.org/10.1016/j.apsusc.2010.10.051
[37] L. Zhu, Q. Lu, L. Lv, Y. Wang, Y. Hu, Z. Deng, Z. Lou, Y. Hou, F. Teng, Ligand-free rutile and anatase TiO_2 nanocrystals as electron extraction layers for high performance inverted polymer solar cells, *RSC Advances* **7** (2017) 20084-20092. https://doi.org/10.1039/C7RA00134G
[38] R. Amadelli, L. Armelao, E. Tondello, S. Daolio, M. Fabrizio, C. Pagura, A. Velichenko, A SIMS and XPS study about ions influence on electrodeposited PbO_2 films, *Applied Surface Science* **142** (1999) 200-203. https://doi.org/10.1016/S0169-4332(98)00707-7

[39] K. S. Kim, T. J. O'Leary, N. Winograd, X-ray photoelectron spectra of lead oxides, *Analytical Chemistry Journal* **45** (1973) 2214-2218. https://doi.org/10. 1021/ac60335a009
[40] M. Sui, S. Kunwar, P. Pandey, J. Lee, Strongly confined localized surface plasmon resonance (LSPR) bands of Pt, AgPt AgAuPt nanoparticles, *Scientific Reports* **9** (2019) 16582. https://doi.org/10.1038/s41598-019-53292-1
[41] J. Zhao, S. Xue, R. Ji, B. Li, J. Li, Localized surface plasmon resonance for enhanced electrocatalysis, *Chemical Society Reviews* **50** (2021) 12070-12097. https://doi.org/10.1039/D1CS00237F
[42] B. Ohtani, K. Iwai, S.-I. Nishimoto, S. Sato, Role of platinum deposits on titanium (IV) oxide particles: Structural and kinetic analyses of photocatalytic reaction in aqueous alcohol and amino acid solutions, *The Journal of Physical Chemistry B* **101** (1997) 3349-3359. https://doi.org/10.1021/jp962060q
[43] E. Fakhrutdinova, O. Reutova, L. Maliy, T. Kharlamova, O. Vodyankina, V. Svetlichnyi, Laser-based synthesis of TiO_2-Pt photocatalysts for hydrogen generation, *Materials* **15** (2022) 7413. https://doi.org/10.3390/ma15217413
[44] A. Hankin, F. E. Bedoya-Lora, J. C. Alexander, A. Regoutz, G. H. Kelsall, Flat band potential determination: avoiding the pitfalls, *Journal of Materials Chemistry A* **7** (2019) 26162-26176. https://doi.org/10.1039/C9TA09569A
[45] S. Trasatti, Electrocatalysis in the anodic evolution of oxygen and chlorine, *Electrochimica Acta* **29** (1984) 1503-1512. https://doi.org/10.1016/0013-4686(84)85004-5
[46] K. S. Exner, H. Over, Beyond the rate-determining step in the oxygen evolution reaction over a single-crystalline IrO_2(110) model electrode: kinetic scaling relations, *ACS Catalysis* **9** (2019) 6755-6765. https://doi.org/10.1021/acscatal.9b01564
[47] A. S. Bolocang, M. J. Phasha, Formation of titanium nitride produced from nanocrystalline titanium powder under nitrogen atmosphere, *International Journal of Refractory Metals and Hard Materials* **28** (2010) 610-615. https://doi.org/10.1016/j.ijrmhm.2010.05.008
[48] Y. B. Egorova, L. V. Davidenko, Titanium alloy strength diagrams at operating temperatures, *Metallurgist* **67** (2023) 614-627. https://doi.org/10.1007/s11015-023-01550-z
[49] O. Shmychkova, D. Girenko, A. Velichenko, Cl^-/ClO^- process on SnO_2-based electrodes in low-concentrated NaCl solutions, *Electrochemical Science Advances* **2** (2022) e2100086. https://doi.org/10.1002/elsa.202100086
[50] O. Shmychkova, D. Girenko, A. Velichenko, Noble metals doped tin dioxide for sodium hypochlorite synthesis from low-concentrated NaCl solutions, *Journal of Chemical Technology & Biotechnology* **97** (2022) 903-913. https://doi.org/10.1002/jctb.6973